ELSEVIER

S0266-3538(96)00005-X

Composites Science and Technology 56 (1996) 439–449

0266-3538/96/$15.00

MEASUREMENT OF MIXED-MODE DELAMINATION FRACTURE TOUGHNESS OF UNIDIRECTIONAL GLASS/EPOXY COMPOSITES WITH MIXED-MODE BENDING APPARATUS

M. L. Benzeggagh & M. Kenane

Université de Technologie de Compiègne, Laboratoire de Génie Mécanique (Polyméres et Composites), LG2ms URA CNRS 1505, BP 649, 60200 Compiègne Cedex, France

(Received 5 January 1995; revised version received 18 September 1995; accepted 14 December 1995)

Abstract

Initiation of cracking and delamination growth in a unidirectional glass/epoxy composite were evaluated under mode I, mode II, and mixed mode I + II static loading. They have been expressed in terms of the total critical strain energy release rate, G_{TC}, and the total fracture resistance, G_{TR}. For the mixed mode I + II, a mixed-mode bending apparatus was used. The loading in this test is a simple combination of the double cantilever beam mode I and the end notch flexure mode II tests. In addition to characterisation of delamination initiation, whatever the value of the G_{II}/G_T modal ratio, this apparatus allows the plotting of an R curve, from which we obtain the total fracture resistance, G_{TR}.

Experimental results were correlated with computations of a semi-empirical criterion through the plotting of the total critical strain energy release rate, G_{TC}, versus the G_{II}/G_T modal ratio, and of the total fracture resistance, G_{TR}, versus the G_{II}/G_T modal ratio.

© 1996 Elsevier Science Limited

Keywords: mode I, mode II, mixed mode, strain energy release, *R* curve, semi-empirical criterion

NOTATION

a_{eff}	Effective crack length
ALDCB	Asymmetrical load double cantilever beam
B	Width of specimen
C	Compliance
CBON	Cantilever beam opening notch
CLS	Cracked lap shear
DCB	Double cantilever beam
EDT	Edge delamination tension
ELS	End loaded split
ENF	End notch flexure
G_{IC}, G_{IIC}, G_{TC}	Mode I, mode II and total critical strain energy release rate
G_{IR}, G_{IIR}, G_{TR}	Mode I, mode II and total fracture resistance
IDCB	Imposed displacement cantilever beam
MMB	Mixed mode bending
MMF	Mixed mode flexure
m_c, m_R	semi-empirical criterion exponents applied to delamination initiation and growth
P_{IC}, P_{IIC}, P_{TC}	Mode I, mode II and total critical loads

1 INTRODUCTION

The delamination process is frequently met in composite materials and in most cases it results from mode I, mode II, or mixed mode I + II delamination. Delamination failure under pure mode I, where DCB testing is commonly used and under pure mode II where ENF and ELS tests are frequently used, have been well studied.[1–3] However, in most realistic situations composite structures are subjected to both modes listed above. For the mixed mode, different specimens have been proposed in the literature, most of which present practical limitations in their use. In fact, some do not permit testing of materials in a large range of mixed-mode ratios, $G_{\text{II}}/G_{\text{T}}$, such as ALDCB,[4,5] MMF,[6–8] and CBON,[9,10] whereas for others, either it is difficult to interpret results, making it necessary to use a finite element analysis such as CLS[11] and EDT,[12] or requiring the use of complex machines (ALDCB). For instance, we may mention the case of the IDCB test,[13] for which it is impossible to plot the *R* curve, since the mixed-mode ratio depends on crack length. Consequently, the MMB test[14] appears to be very interesting for testing materials in mixed mode because it allows characterisation of the delamination initiation and growth for any value of the $G_{\text{II}}/G_{\text{T}}$ modal ratio.

The present study concerns the characterisation of delamination initiation and growth on the basis of a strain energy release rate concept. In addition to mode I and mode II, we have studied six G_{II}/G_T modal ratios. For each G_{II}/G_T ratio several specimens were tested. Good agreement was obtained between experimental results for G_{TC} and G_{TR}, and calculations of a semi-empirical criterion.[15] For the G_{TC} versus G_{II}/G_T modal ratio we found $m_{TC} = 2{\cdot}6$, but for the G_{TR} versus G_{II}/G_T modal ratio we found $m_{TR} = 1$. The latter corresponds to the classical criterion.

2 RESULTS AND DISCUSSION

2.1 Material

The material used in this study was an M10 epoxy resin (Vicotex) reinforced with 52% by volume of E-glass fibres, 5% of which are woven perpendicularly. This material was prepared in the form of compression-moulded, 6 mm thick panels. The crack starter was formed by inserting a Teflon film at mid-thickness during moulding.

The elastic constants obtained experimentally[16] were:

$E_{11} = 36{\cdot}2$ GPa $\quad G_{12} = 5{\cdot}6$ GPa $\quad \nu_{12} = 0{\cdot}26$

$E_{22} = 10{\cdot}6$ GPa $\quad G_{13} = 3{\cdot}7$ GPa $\quad \nu_{13} = 0{\cdot}33$

$E_{33} = 7{\cdot}2$ GPa $\quad G_{23} = 3{\cdot}2$ GPa $\quad \nu_{23} = 0{\cdot}48$

2.2 Specimens

The following test specimens were subjected to monotonic flexural loading:

- In pure mode I, a DCB (Fig. 1(a)).
- In pure mode II, an ELS (Fig. 1(b)).

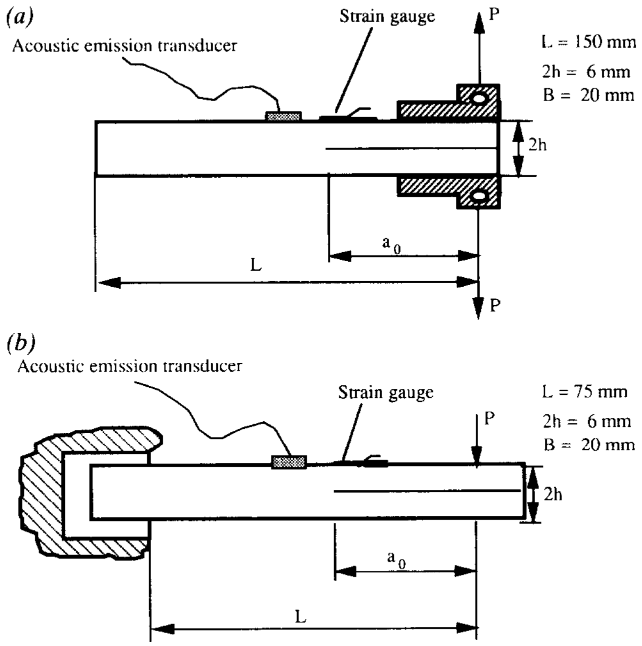

Fig. 1. (a) DCB specimen; (b) ELS specimen.

- In mixed mode, an MMB specimen proposed by Crews *et al.* and adapted to our material by Aboura *et al.*[17] based on the work of Reeder *et al.*[18] This is a simple combination of a DCB (mode I) specimen and an ENF (mode II) specimen (Fig. 2). Load is applied to a split-beam specimen by means of a lever where the distance, e, between the load point and the fulcrum can be varied. The design of the MMB apparatus allows us to introduce mode I loading at the end of the lever and mode II loading at the fulcrum.

2.3 Test conditions

All tests were performed in an Instron machine at 2 mm/min constant displacement rate. In order to study the damage initiation mechanisms and crack propagation, a strain gauge was bonded to each specimen. An acquisition system permits simultaneous recording of the load, P, the displacement, δ, the response of the strain gauge and the acoustic emission from the loaded sample.

2.4 Measurement of G_{TC} and G_{TR}

The total critical strain energy release rate, G_{TC}, was determined experimentally by the Irwin–Kies compliance method:

$$G_{TC} = \frac{P_{TC}^2}{2B}\frac{dC}{da} \tag{1}$$

2.4.1 Compliance

The compliance of a composite material in mode I when using a DCB specimen is given by $C = a^n/h$, where n and h are empirical constants for the laminates under consideration.

In the case of mode II and mixed-mode I + II, the compliance is $C = \alpha + \beta a^3$, where α and β are empirical constants that depend on the G_{II}/G_T modal ratio. The compliances for different G_{II}/G_T modal ratios considered in this study were computed (Fig. 3). We have observed that the compliance increases when the G_{II}/G_T modal ratio decreases.

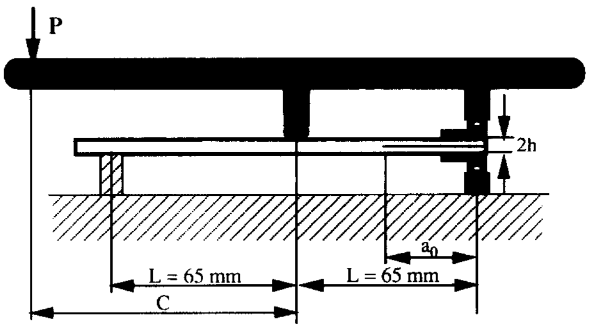

Fig. 2. MMB apparatus.

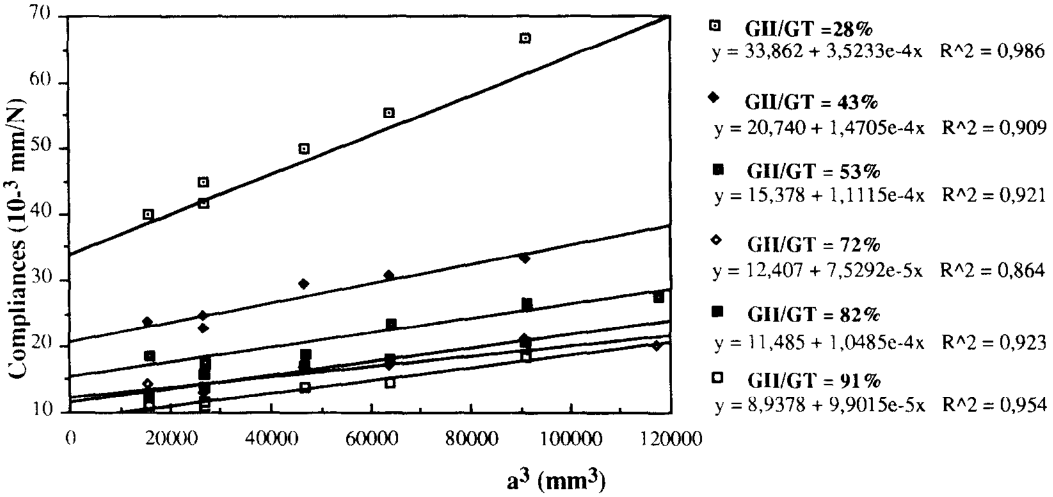

Fig. 3. Compliance, C, versus a^3.

2.4.2 Total critical energy, G_{TC}

The simultaneous recording of the load, the displacement of the load application point, the response of the strain gauge, and the acoustic emission allows us to detect precisely the critical point, A (P_{TC}, δ_{TC}), which is necessary to determine G_{TC}. Many studies[6,9,19] have shown that this method is more useful than 'visual assessment' (as defined in the new ASTM standard 05528–94a).

Table 1 summarises the results of the G_{TC} values as

Table 1. Results of strain energy release rates G_{IC}, G_{IIC}, and G_{TC}

e^a (mm)	G_{II}/G_T (%)	a_0 (mm)	P_{TC} (N)	G_{TC} (J/m^2)	e (mm)	G_{II}/G_T (%)	a_0 (mm)	P_{TC} (N)	G_{TC} (J/m^2)
Mode II	100	30	600·59	2494·78	50	53	24	349·43	554·44
	100	41	489·5	3029·44	50	53	24	376·53	675·78
	100	41	493·77	3147·92	50	53	25	359·5	638
	100	42	477·9	3094·42	50	53	25	314·88	504·78
	100	50	366·82	2762·23	50	53	25·5	327·7	540·76
					50	53	26	322·75	563·96
	$G_{IIC} = 2905·76 \pm 224·55$ (J/m^2)					$G_{TC} = 579·62 \pm 58·66$ (J/m^2)			
30	91	23	785·89	2428·34	60	43	24·5	258·42	433·07
30	91	24·5	751·71	2351·47	60	43	25	298·28	569·76
30	91	25	773·19	2591·98	60	43	26	282·04	527·05
30	91	25·5	757·08	2675·04	60	43	31·5	258·67	697·1
	$G_{TC} = 2457·26 \pm 100·30$ (J/m^2)					$G_{TC} = 568·36 \pm 98·58$ (J/m^2)			
35	82	24·5	656·62	1950·27	90	28	23	149·11	307·43
35	82	25	601·81	1688·03	90	28	23·5	150·46	323·6
35	82	25	612·06	1798·85	90	28	25	141·43	319·65
35	82	27·5	550·78	1849·18	90	28	25·5	143·25	339
35	82	32	486·08	1823·30	90	28	28·5	143·80	412·09
	$G_{TC} = 1821·93 \pm 84·47$ (J/m^2)					$G_{TC} = 340·35 \pm 37·26$ (J/m^2)			
40	72	24	518·43	827·78	Mode I	0	23	57·69	121·41
40	72	24·5	514·4	866·57		0	41	43·48	113·4
40	72	25	607·91	1243·27		0	45	44·75	116·83
40	72	25	530·4	927·34		0	46	43·33	119·23
40	72	27·5	509·03	1068·59		0	55	28·61	119·23
40	72	31·5	482·06	1268·47					
	$G_{TC} = 1033·67 \pm 174·11$ (J/m^2)					$G_{IC} = 118·02 \pm 02·72$ (J/m^2)			

^{a} See Fig. 2.

a function of crack length and G_{II}/G_T modal ratio. The results show a logical development. The higher the G_{II}/G_T modal ratio, the greater the value of G_{TC}.

We have observed that there is a large difference between values of G_{IC} and of G_{IIC}: this corresponds specifically to the behaviour of composites consisting of a brittle matrix.[20]

2.4.3 *Total fracture resistance, G_{TR}*

The different compliance laws corresponding to G_{II}/G_{TC} modal ratio values considered in this study allowed us to plot the *R* curves. These show the variation in total fracture resistance, G_{TR}, as the delamination extends.

The following equations permit computation of a_{eff}. From the compliance, *C*, for mode I:

$$C = \frac{a_{eff}^n}{h} = \frac{\delta_{IR}}{P_{IR}}$$

which yields:

$$a_{eff} = \left(h\frac{\delta_{TR}}{P_{TR}}\right)^{1/n} \quad (2)$$

For mode II and mixed mode:

$$C = \alpha + \beta a_{eff}^3 = \frac{\delta_{TR}}{P_{TR}}$$

From these we obtain:

$$a_{eff} = \sqrt[3]{\frac{\frac{\delta_{TR}}{P_{TR}} - \alpha}{\beta}} \quad (3)$$

Thus, the total fracture resistance during crack growth is expressed as:

$$\text{Mode I: } G_{TR} = \frac{nP_{TR}^2 a_{eff}^{n-1}}{2Bh} \quad (4)$$

$$\text{Mode II and mixed mode: } G_{TR} = \frac{3P_{TR}^2}{2Bh}\beta a^2 \quad (5)$$

The *R* curve method allows the strain energy release rate to increase with crack length, reaching a plateau for $a_{eff} \geq 50$ mm (Fig. 4) corresponding to G_{IR}, G_{IIR} and G_{TR}, as appropriate.

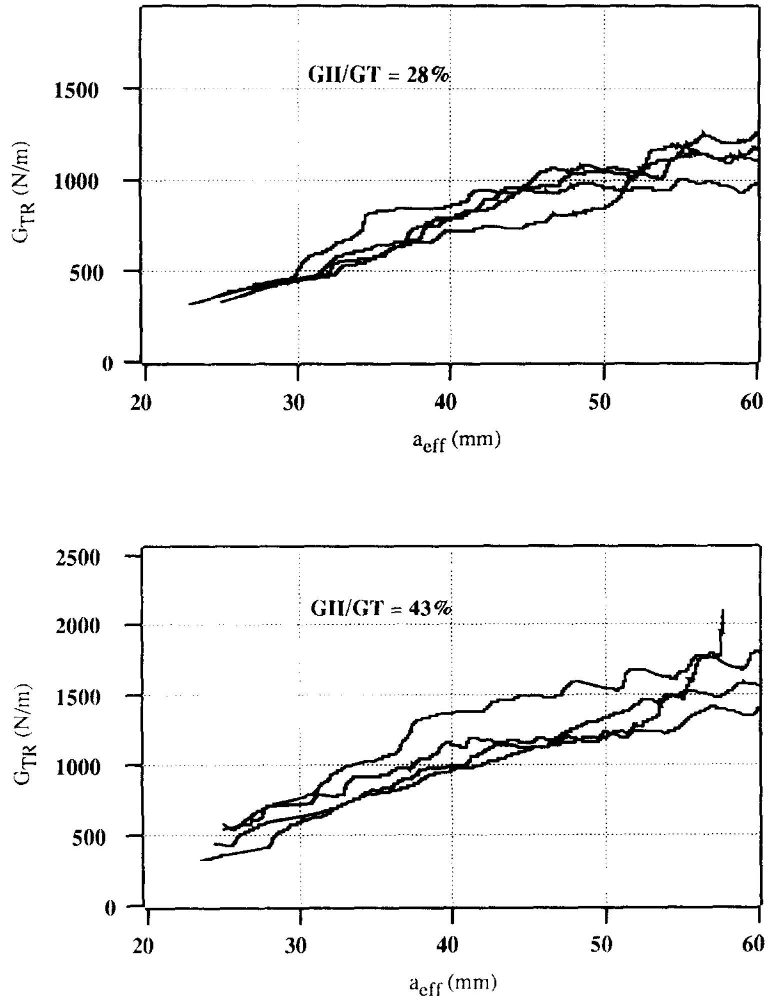

Fig. 4. G_{TR} versus effective crack length, a_{eff}.

Figure 4 shows examples of R curves for two mixed-mode ratios, $G_{II}/G_T = 28$ and 43%, obtained from eqns (2)–(5).

The variation of G_{TR} with G_{II}/G_T modal ratio is related to the fracture mechanisms dissipating the energy taken into account according to the G_{II}/G_T modal ratio considered. Before interpreting the rupture mechanisms it is interesting to show the changes in the load/displacement curves which progressively change from the mode I curve form to the mode II curve form, according to the G_{II}/G_T modal ratio value (Fig. 5). In fact, for pure mode I the load increases continually from the point of damage initiation, A (Fig. 5(a)), and then reaches a plateau where the load is almost constant. At $G_{II}/G_T = 28\%$, the load increases in a single stage before starting a

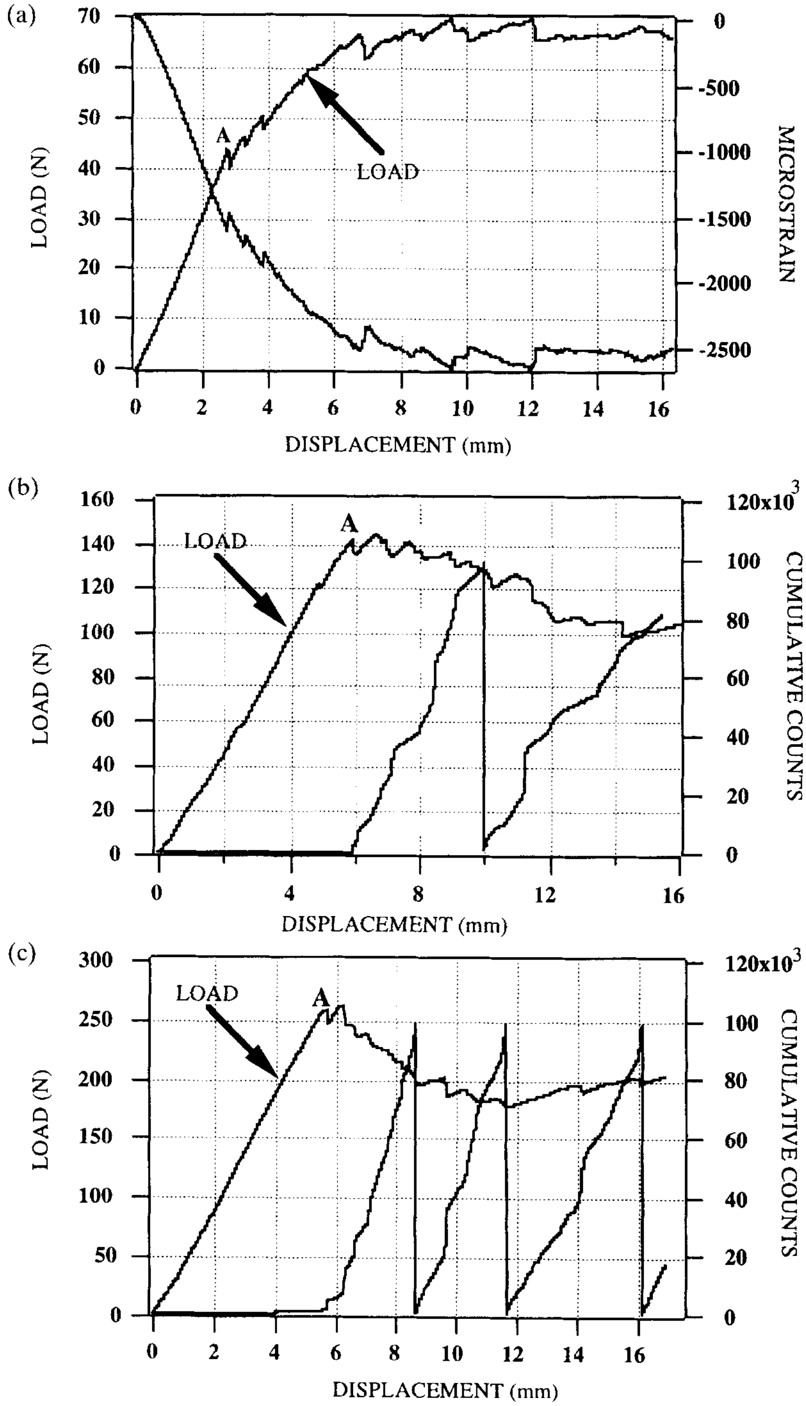

Fig. 5. (a) Load and micro-strain versus displacement, mode I; (b) load and cumulative counts versus displacement, G_{II}/G_T =28%; (c) load and cumulative counts versus displacement, $G_{II}/G_T = 43\%$; (d) load and cumulative counts versus displacement, $G_{II}/G_T = 53\%$; (e) load and micro-strain versus displacement, $G_{II}/G_T = 72\%$; (f) load and cumulative counts versus displacement, $G_{II}/G_T = 91\%$; (g) load and micro-strain versus displacement, mode II.

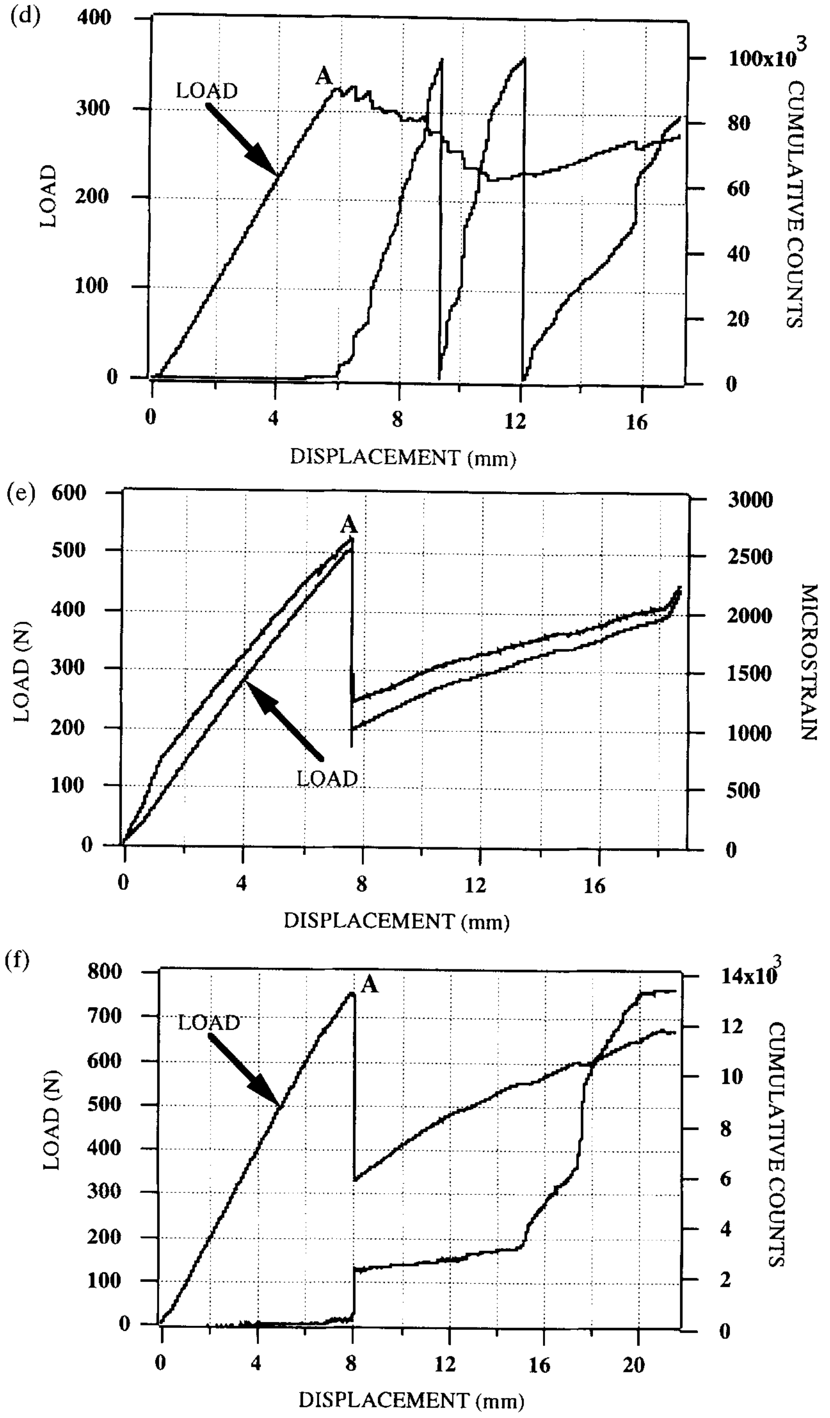

Fig. 5.—*Contd.*

progressive decrease with a low slope (Fig. 5(b)). In the case of $G_{II}/G_T = 43\%$, this load decrease becomes more pronounced after the damage initiation point (Fig. 5(c)). When the participation rate of mode I and mode II are the same ($G_{II}/G_T = 53\%$), we notice the appearance of a slight instability of the load after the damage initiation point characterising a more substantial participation of mode II compared to previous cases (Fig. 5(d)). For $G_{II}/G_T = 72\%$ (Fig. 5(e) and (f)), an important drop in the load occurs just after the point of damage initiation. This is a characteristic of the propagation instability phenomenon noticed generally in pure mode II (Fig. 5(g)). This propagation instability raises the difficulty of the total fracture resistance measurement as we approach pure mode II. For the $G_{II}/G_T = 82\%$ case, all the curves exhibit drastic drops after initiation of the delamination process, which characterises unstable propagation. In this case, if we consider $G_{TR} = G_{TC}$ we note that we underestimate the total fracture resistance compared to the other modal ratios that we studied. There is only one curve that presents a plateau

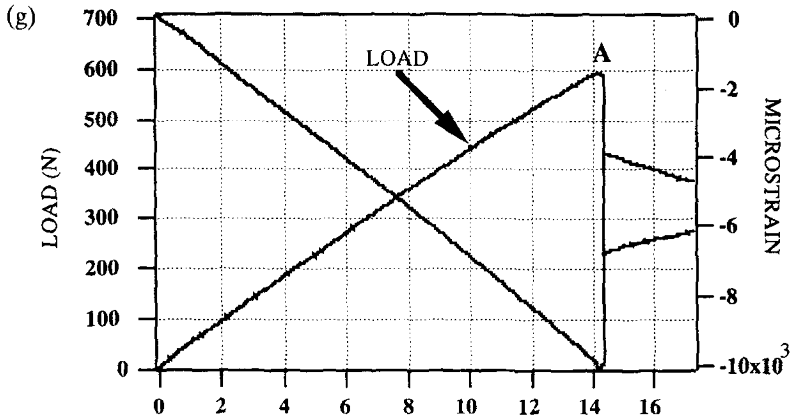

Fig. 5.—*Contd.*

permitting measurement of the total fracture resistance for which the value is acceptable.

Table 2 lists the experimentally obtained results for G_{IR}, G_{IIR}, and G_{TR}.

2.5 Fractographic analysis

In order to understand the interlaminar fracture mechanisms, the fracture surfaces were examined in a scanning electron microscope (SEM). It was observed that pure mode I is characterised by fractures localised principally in the resin and along the resin/fiber interface (Fig. 6). By contrast, pure mode II is characterised by fractures localised in the resin with many hackles having an orientation of approximately 45° with respect to the fiber direction (Fig. 7), which for mode II loading is the principal normal stress plane.[21]

In the case of mixed mode, the mechanisms are more complex.[22,23] Figure 8 shows a fracture surface corresponding to $G_{II}/G_T = 28\%$. As we see, the

Table 2. Experimental results of the fracture resistances G_{IR}, G_{IIR}, and G_{TR}

e^a (mm)	G_{II}/G_T (%)	G_{TR} (J/m^2)	e (mm)	G_{II}/G_T (%)	G_{TR} (J/m^2)
Mode II	100	2494·78	50	53	1825
	100	3029·44	50	53	1803
	100	3147·92	50	53	1772
	100	3094·42	50	53	1500
	100	2762·23	50	53	1863
$G_{IIR} = 2905{\cdot}76 \pm 244{\cdot}55$ (J/m^2)			$G_{TR} = 1752{\cdot}60 \pm 129{\cdot}73$ (J/m^2)		
30	91	2428·34	60	43	1500
30	91	2351·47	60	43	1558
30	91	2591·98	60	43	1200
30	91	2675·04	60	43	1500
$G_{TR} = 2457{\cdot}26 \pm 100{\cdot}30$ (J/m^2)			$G_{TR} = 1439{\cdot}50 \pm 140{\cdot}29$ (J/m^2)		
35	82	2625	90	28	1300
			90	28	1073·5
			90	28	1100
			90	28	100
$G_{TR} = 2625{\cdot}00 \pm 0$ (J/m^2)			$G_{TR} = 1118{\cdot}37 \pm 111{\cdot}07$ (J/m^2)		
40	72	1900	Mode I	0	370
40	72	1880		0	430
40	72	2260		0	490
40	72	2227		0	425
$G_{TR} = 2066{\cdot}75 \pm 177{\cdot}27$ (J/m^2)			$G_{IR} = 428{\cdot}75 \pm 42{\cdot}48$ (J/m^2)		

^{a} See Fig. 2.

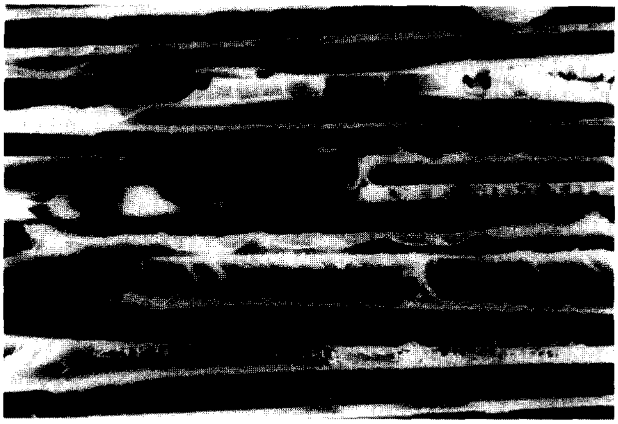

Fig. 6. Mode I fracture surface (presence of cleavage paths).

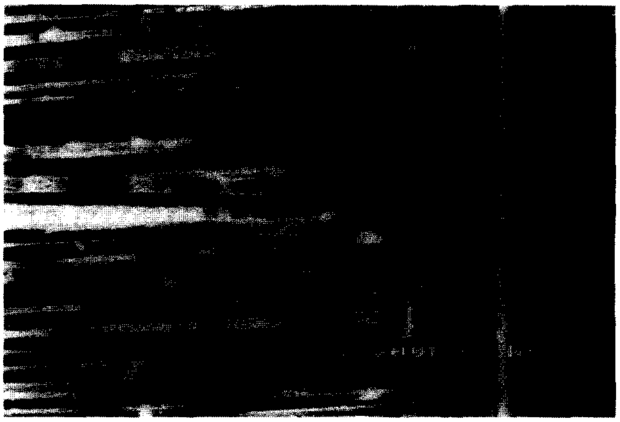

Fig. 8. Mixed-mode fracture surface, $G_{II}/G_T = 28\%$.

fracture surface exhibits cleavage paths characterising the opening mode. It also shows hackles oriented at less than 45° with respect to the fracture surface. These hackles are mainly forward as a consequence of matrix shear rupture caused by the participation of mode II. Some of the hackles are fractured by mode I at their base on the rupture surface (Fig. 9). This results in the presence of traces displaying a river-like form. As the participation of mode II increases, more developed shear hackles are observed and the cleavage paths are less frequent (Fig. 10).

2.6 Reflection on the application of a semi-empirical criterion

In order to predict G_{TC} and G_{TR} as functions of G_{II}/G_T modal ratio, the following relationship is suggested:

$$G_{TC} = G_{IC} + (G_{IIC} - G_{IC})\left(\frac{G_{II}}{G_T}\right)^m$$

On the other hand, it is interesting to know how G_{TR} increases independently of G_{TC} as a function of G_{II}/G_T. The experimental measurements of G_{TC} are thus presented as a function of G_{II}/G_T modal ratio in Fig. 11. Figure 12 shows the mode I energy contribution versus the mode II energy component. The application of this semi-empirical criterion gives good results for $m_c = 2{\cdot}6$:

$$G_{TC} = 118{\cdot}31 + 2795{\cdot}18\left(\frac{G_{II}}{G_T}\right)^{2{\cdot}6}$$

Fig. 9. Mixed-mode fracture surface, $G_{II}/G_T = 72\%$. A indicates cleavage path traces resulting from hackles fractured by mode I.

Fig. 7. Mode II fracture surface (presence of shear hackles).

Fig. 10. Mixed-mode fracture surface, $G_{II}/G_T = 91\%$.

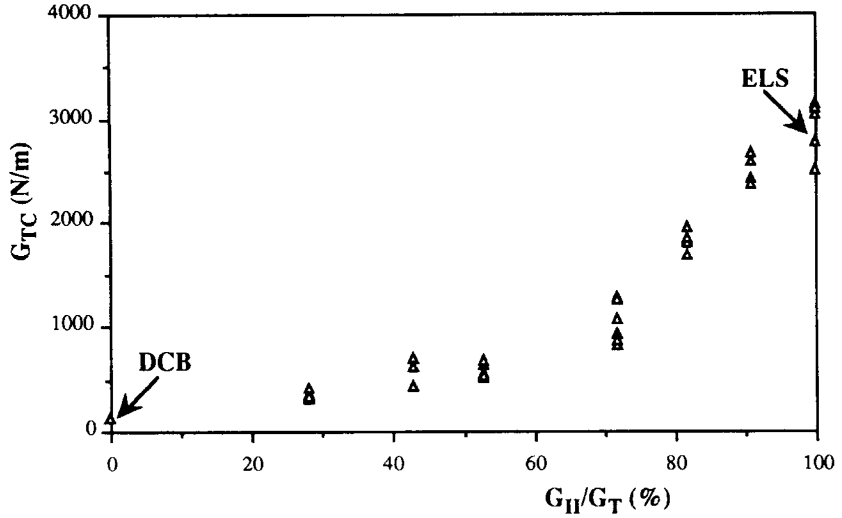

Fig. 11. G_{TC} versus G_{II}/G_T modal ratio.

From experiment: $G_{IC} = 118{\cdot}02$ J/m^2; $G_{IIC} = 2905{\cdot}76$ J/m^2; $G_{IIC} - G_{IC} = 2787{\cdot}74$ J/m^2. We see that the curve $G_{TC} = f(G_{II}/G_T)$ is composed of three stages:

- a first stage, $0\% \leq G_{II}/G_T \leq 53\%$, where G_{TC} increases progressively when the G_{II}/G_T modal ratio increases;
- a transition stage, $53\% \leq G_{II}/G_T \leq 72\%$, where the curve takes a large radius towards higher energy values than in previous cases; this is due to the fact that the mode II ratio is becoming important;
- a final stage, $72\% \leq G_{II}/G_T \leq 100\%$, where the energy values were comparable to the pure mode II values.

Practically the same m parameter value ($m_c = 2$) has been obtained with experimental IDCB results.[24] This method does not permit the measurement of G_{TR} because the G_{II}/G_T ratio depends on the crack length. For this purpose, we have used the MMB apparatus.

In Fig. 13 are plotted values of G_{TR} versus the G_{II}/G_T modal ratio. The correlation between the experimental values of G_{TR} and the semi-empirical calculations appears to be better than the case of G_{TC} with $m_R = 1$, and have used the classical criterion used widely in the literature:

$$G_{TR} = 419{\cdot}21 + 2408{\cdot}34\left(\frac{G_{II}}{G_T}\right)^1$$

From experiment: $G_{IR} = 428{\cdot}75$ J/m^2; $G_{IIR} = 2905{\cdot}76$ J/m^2; $G_{IIR} - G_{IR} = 2477{\cdot}01$ J/m^2.

Figure 14 shows the mode I fracture resistance contribution versus the mode II component.

It appears to us that the m parameter (m_c, m_R) permits us to distinguish between the changes in G_{TC} and G_{TR} as functions of the G_{II}/G_T modal ratio. In order to verify the generality of the criterion, studies on woven composites[25] have shown that the m parameter depends on whether the resin is brittle ($m_c = 2$) or ductile ($m_c = 3$), but it is independent of

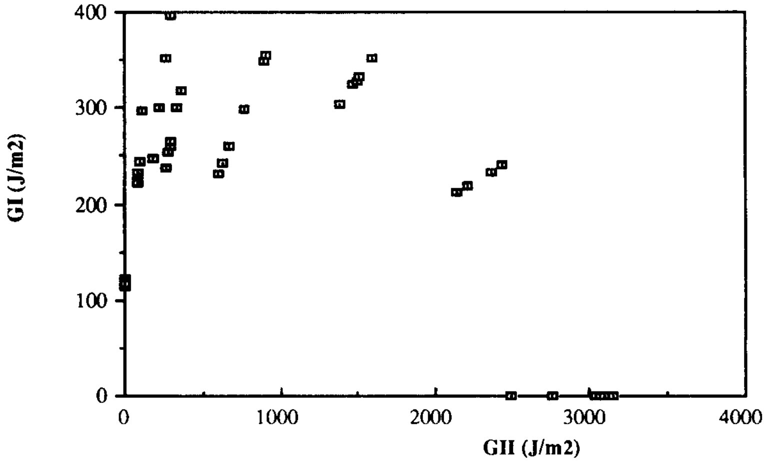

Fig. 12. Mode I energy contribution, G_I, versus mode II energy component, G_{II}.

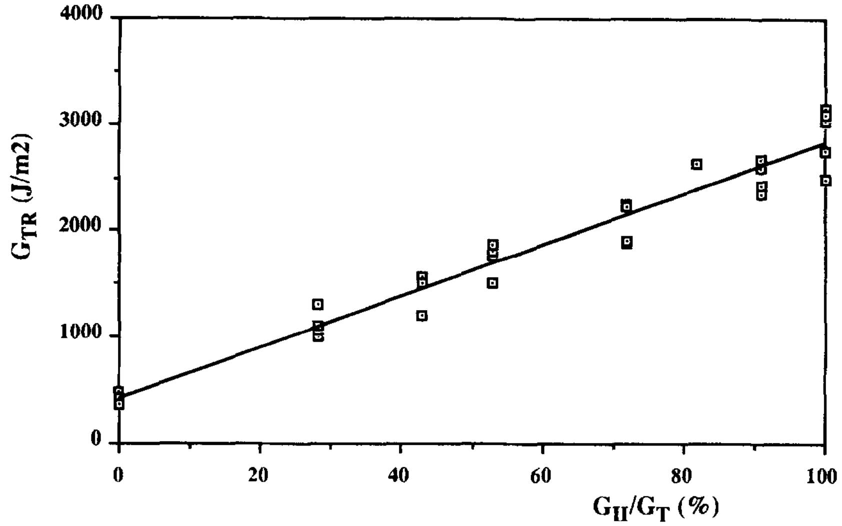

Fig. 13. G_{TR} versus G_{II}/G_T modal ratio.

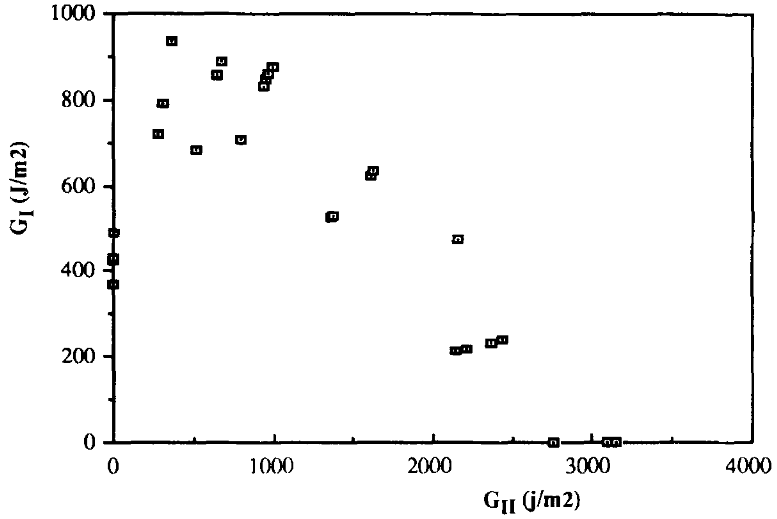

Fig. 14. Mode I fracture resistance contribution versus mode II component, G_{II}

the displacement rate of loading. However the criterion provides a good fit to the delamination initiation results for carbon-fibre/epoxy composites,[26] with m_c taking the value of 1·557.

3 CONCLUSIONS

- The MMB apparatus appears to be very easy in use. It simulates perfectly the mixed-mode delamination, and permits computation of G_{TR} and therefore the R curve for any G_{II}/G_T modal ratio value.
- We have shown that the form of the curve is characteristic of the mixed-mode ratio considered.
- Good agreement was found between the experimental results and calculations of a semi-empirical criterion. In fact, G_{TC} increases as a function of G_{II}/G_T with $m_c = 2{\cdot}6$, whereas G_{TR} versus G_{II}/G_T modal ratio is linear with $m_R = 1$.

REFERENCES

1. Russel, A. J. & Street, K. N., Moisture and temperature effects on the mixed mode delamination fracture in graphite/epoxy. ASTM STP 876, 1985, pp. 349–70.
2. Benzeggagh, M. L., Prel, Y. J. & De Charentenay, F. X., Experimental analysis of mode I delamination testing. 5th Int. Conf. on Composites Materials, ICCMV, San Diego, CA.
3. Prel, Y., Benzeggagh, M. L. & Roedlandt, J. M., Étude par élément finis et corrélation expérimentale du délaminage en mode I et en mode II. *JNC5*, Paris, 1986, pp. 49–62.
4. Vanderkley, P. S., Mode I–mode II delamination

fracture toughness of a unidirectional graphite/epoxy composite. Masters thesis, Texas, 1981.
5. Bradley, W. L. & Cohen, R. N., Matrix deformation and fracture in graphite reinforced epoxies. *Delamination and Debonding of Materials*. ASTM STP 876, Philadelphia, PA, 1985, pp. 389–410.
6. Benzeggagh, M. L., Gong, X. J. & Roedlandt, J. M., A mixed mode delamination specimen and its finite element analysis. *ICCM 7*, China, 1989, p. 210.
7. Davies, P., Comportement en délaminage des matériaux composites à matrice thermoplastiques. Doctoral thesis, UTC, 1987.
8. Hashemi, S., Kinloch, A. J. & Williams, J. G., The effects of geometry, rate and temperature on the mode I, mode II and mixed mode I + II interlaminar fracture of carbon fiber/poly(ether ketone) composites. *J. Comp. Mater.*, **24** (1990) 918–56.
9. Benzeggagh, M. L., Gong, X. J., Davies, P., Roedlandt, J. M., Mourin, Y. & Prel, Y. A mixed mode specimen for interlaminar fracture testing. *Comp. Sci. Technol.*, **34** (1989) 129–143.
10. Benzeggagh, M. L., Gong, X. J. & Roedlandt, J. M., Rupture interdélaminatoire en mode mixte I + II. *JNC6*, Paris, 1988, pp. 365–77.
11. Ramkumar, R. L. & Whitcomb, J. D., Characterization of mode I and mixed mode delamination growth in T300/5028 graphite epoxy. ASTM STP 876, 1985, pp. 315–35.
12. O'Brien, T. K., Characterization of delamination onset and growth in composite laminate. ASTM STP 775, 1982, pp. 140–57.
13. Gong, X. J. & Benzeggagh, M. L., Determination of the mixed mode delamination toughness using an imposed displacement cantilever beam test method, *ECCM 5*, Bordeaux, 1992.
14. Crews, J. H. & Reeder, J. R., A mixed mode bending apparatus for delamination testing. NASA TM 100662 Report, 1988.
15. Gong, X. J. & Benzeggagh, M. L., Mixed mode interlaminar fracture toughness of unidirectional glass/epoxy composite. ASTM STP 1230, 1995, pp. 100–23.
16. Gong, X. J., Rupture interlaminaire en mode mixte I + II du composite stratifié verre/epoxy unidirectionnel et multidirectionnel. PhD thesis, Université de Technologie de Compiègne, 1992.
17. Aboura, Z., Gong, X. J., Sastra, Y. H. & Benzeggagh, M. L., Étude comparative entre deux tests de mode mixte I + II introduisant des géométries d'éprouvettes de types IDCB et MMB. *JNC 8*, Paris, 1992, pp. 679–90.
18. Reeder, J. R. & Crews, J. H., Non-linear analysis and redesign of the mixed mode bending delamination test. NASA TM 102777, 1991.
19. Laksimi, A., Benzeggagh, M. L., Gong, J., Hecini, M. & Roelandt, J. M., Mode I interlaminar fracture of symmetrical cross-ply composites. *Comp. Sci. Technol.*, **41** (1991) 147–64.
20. Friedrich, K., Fracture analysis of polymer composites. In *Composite Materials Sciences*, Vol. 6, ed. K. Friedrich, 1989, pp. 425–87.
21. Corleto, C., Bradley, W. & Henriksen, M., Correspondence between stress fields and damage zones ahead of crack tip of composites under mode I and mode II loading. *Proc. 6th Int. Conf. on Composite Materials, ICCM and ECCM*. Elsevier, London, 1987.
22. Arcan, L., Arcan, M. & Danieli, M., SEM fractography of pure and mixed mode interlaminar fractures in graphite/epoxy composites. *Fractography of Modern Engineering Materials: Composites and Metals*, ed. J. E. Masters & J. J. Au. ASTM STP 948, 1987, pp. 41–67.
23. Hibbs, M. F. & Bradley, W. L., Correction between micromechanical failure processes and the delamination toughness of graphite/epoxy systems. *Fractography of Modern Engineering Materials: Composites and Metals*, ed. J. E. Masters & J. J. Au. ASTM STP 948, 1987, pp. 68–97.
24. Benzeggagh, M. L., Gong, X. J., Aboura, Z. & Sastra, H. Y., Mixed mode delamination in unidirectional glass/epoxy composites under static and fatigue loading. *ICCM IX*, Madrid, 1992.
25. Aboura, Z., Etude du processus de délaminage mode I, mode II et mode mixte I + II de matériaux composites à renforts tissée à différentes vitesses de sollicitation. PhD thesis, Université de Technologie de Compiègne, 1993.
26. Singh, S. & Partridge, I. K., Delamination failure in unidirectional carbon fibre/epoxy under mixed mode loading. *Polym. & Polym. Comp.* (submitted).